Evaluation of polyacrylate latex nanodispersions efficacy as consolidation agents of porous sandstones using synchrotron micro-computed tomography

Irena Adámková[a], Radek Ševčík[a*], Jana Machotová[b], Lucie Zárybnická[a], Petra Mácová[a], Lucia Mancini[c], Alberto Viani[a,c]

[a] Institute of Theoretical and Applied Mechanics of the Czech Academy of Sciences, Centre Telč, Prosecká 809/76, 190 00 Praha 9, Czech Republic.

[b] Institute of Chemistry and Technology of Macromolecular Materials, Faculty of Chemical Technology, University of Pardubice, Studentská 573, 532 10 Pardubice, Czech Republic

[c] Slovenian National Building and Civil Engineering Institute, Dimičeva ulica 12, SI 1000 Ljubljana, Slovenia.

***Corresponding author**: Dr. Radek Ševčík (E-mail: sevcik@itam.cas.cz)

Abstract

Two concentrated innovative aqueous polyacrylate latex nanosuspensions with and without fluorination have been designed as consolidation agents and tested on two types of highly porous sandstones, namely, Prague (Mšené) and Oberkirchen – building materials of valuable objects of Cultural Heritage. To evaluate the effectiveness of the treatments it is desirable to obtain as much quantitative information as possible and adopt non-invasive analytical techniques. This approach is nowadays possible thanks to recent advances in micro-computed tomography. By means of synchrotron radiation X-ray micro-computed tomography, it has been possible to detect the presence of polymer in the whole sample thickness (4 mm) with a higher concentration close to the surface of the application.

Quantitative image analysis revealed significant differences in total porosity, pore surface area per unit volume and fractal dimension. For example, porosity values were found about 7% and 3% lower in the consolidated Prague and Oberkirchen sandstones, respectively, with a shift towards smaller pores and pore connectivity more pronounced for the Prague sandstone. The adoption of tools for modelling of water transport, based on the retrieved stone pore network, evidenced a decrease in water permeability and diffusivity of more than one order of magnitude in the treated samples, which was more pronounced along the direction of penetration of the consolidating agent. All in all, both latexes exhibited similar film-forming and pore-filling abilities. The effect of the treatment was different between the two stones as a consequence of their different characteristics of the pore network. In general, the presented investigation highlights the huge potential of micro/computed tomography for the quantitative assessments of the porous microstructure of building materials.

Keywords: Consolidation; micro-computed tomography, sandstone; nanodispersion; acrylic latex; microstructure; permeability

1. Introduction

Several solutions have been proposed to protect Cultural Heritage buildings or monuments from the aggressive action of our environment [1]. In the case of natural stone materials, this proved to be a challenging task, because of their different mineralogical composition and microstructure, which dictate their sensitivity to the chemical, physical and biological processes of decay [1]. Nonetheless, consolidating and conservative treatments are frequently deemed necessary [2,3]. The consolidation is aimed at the improvement of the stone cohesion [4], whereas conservation addresses the aspects connected with the protection

of the stone from further damage. Since water is directly or indirectly involved in many forms of stone deterioration, one of the most sought property of protective coatings is water repellency or hydrophobicity [5,6]. Such effects have been obtained in different ways, *e.g.* by adopting alkoxysilanes, silicones and fluoropolymers [7–13].

In this respect, acrylic polymers offer the advantage of high flexibility, because their properties can be tailored to the specific substrate and method of application by resorting to structural modifications during the process of synthesis. Acrylic polymers can be obtained as water-borne dispersions (latexes) composed of particles a few hundreds of nm in size through the environmentally friendly process of emulsion polymerization [14–16]. This approach can be successfully adopted to produce partially fluorinated polyacrylate latexes, which exhibit hydrophobic properties, along with chemical, thermal and photo-oxidative stability, thanks to the high energy of the C–F bond and the high electronegativity of the F atom [17,18]. The impact on costs of the fluorinated latex copolymers can be effectively reduced by preparing them as core-shell particles, without detriment to the properties [19–22]. Moreover, the water resistance of the latex coating film can be improved by covalent cross-linking [23–25], which involves the establishment of inter-molecular chemical bonds, leading to the connection of the latex particles during the film formation.

Crucial to the evaluation of the effectiveness of a consolidation treatment is the description of the spatial distribution of the consolidating agent within the stone [26]. Sample observation with optical and electron microscope is frequently insufficient at the scope, because of the lack of 3D capability and of a reliable quantitative approach. The potential of X-ray microcomputed tomography (mCT) to overcome these difficulties, has been recognized already more than 15 years ago [27,28]. However, it is only recently that, thanks to the development of dedicated software for image analysis, mCT has become a powerful tool for quantitative analysis in a full 3D fashion [29,30]. Nonetheless, the investigation of the

distribution of polymeric compounds within a porous stone is hampered by their low attenuation coefficient for X-rays. A proposed solution to this problem, the consolidants doped with contrast agents have been tested [31,32]. Unfortunately, such an option hides pitfalls, *e.g.* altered penetration ability of the consolidation agent [31].

In this study, we report two examples of consolidation treatment performed on two sandstones with different physical characteristics, by adopting two distinct latex types (fluorinated and non-fluorinated polyacrylate latexes with covalent crosslinking), specifically synthesized for the consolidation of stone. Taking advantage of the peculiar characteristics of the X-rays generated by the synchrotron radiation, and thanks to the adoption of the propagation-based phase-contrast mode [33], which find its natural application with synchrotron-generated X-rays, the visibility of features with similar linear attenuation coefficients, namely, the polymer and the voids, is greatly enhanced. This allows to segment out the polymer from the pore-stone matrix, increasing the accuracy of the description of the pore network and, consequently, the detection of the changes induced by the consolidation treatment. The volume distribution of acrylic latex and the effect of the treatments are described with several quantitative parameters, including the simulation of fluid penetration.

2. Materials and methods

Monomers employed in the synthesis of acrylic latexes, namely, methyl methacrylate (MMA), butyl acrylate (BA), 2,2,2- trifluoroethyl methacrylate (TFEMA), methacrylic acid (MAA), allyl methacrylate (ALMA), and diacetone acrylamide (DAAM), were purchased from Sigma-Aldrich (Czech Republic). Ammonium persulfate (Penta, Czech Republic) was used as the initiator, whereas Disponil FES 993 (BASF, Czech Republic) was employed as an emulsifier. Adipic acid dihydrazide (ADH) was used as a crosslinking agent and was purchased from TCI Europe (Switzerland).

2.1 Stone samples

As the first example of porous sandstone, Prague (Mšené) sandstone (PS) was selected. This stone is described in the literature as a fine-grained white-grey rock composed of about 95% of sub-oval quartz clasts and it contains minor clay fractions (mainly kaolinite) and accessory minerals, such as tourmaline, epidote, muscovite and zircone [34,35]. Sandstone is excavated in a quarry near Mšené-lázně (Czech Republic), a town north-west of the city of Prague (Czech Republic), and it has been employed in the construction of many historical buildings, such as the famous St. Vitus's Cathedral, dominating the historical center of the capital city. Its use continued over time and nowadays it is still adopted in restoration works [35]. The porosity has been reported to range between 26.3 and 29.7 vol.% [34]. The unimodal pore size distribution peaked at 30 μm, with the major amounts of pores with diameters ranging from 20 to 40 μm [36].

As the second sample, the Oberkirchen sandstone (OS) quarried in Bückeberge (Germany) was applied. It is a white-grey to light orange rock composed of quartz (~ 98%) with minor amounts of feldspars, dolomite, opaque minerals and kaolinite. Kaolinite and dolomite are frequently "bridging" quarts grains within the matrix [37]. This stone has been extensively used in building construction; notable examples are the Royal palace in Amsterdam (Netherlands), the St Martin`s Tower in Groningen (Netherlands) and the town hall of Antwerp (Belgium). The quarry is still in operation. The porosity is typically in the range of 16.4 – 20.6%, with values of average pore diameter and median pore diameter of 0.8 μm and 11.1 μm, respectively [37,38].

2.2 Synthesis of polyacrylate latexes

Two polyacrylate latexes were synthesized: a fluorine-free composition, labelled A, and a fluorinated composition, labelled B. Following a common preparation route for fluorine-containing or reactive latex compositions, a two-step synthesis strategy was adopted. During

the first step, a seed latex, or ‘core’, based on general acrylic monomers, is obtained. In the second step, the fluorinated or special monomers are copolymerized with the general monomers to form a ‘shell’ [20,22,39–43]. In latex B, TFEMA was copolymerized with the monomers of the second step, in the amount of 45 wt.%. Both A and B latexes implemented covalent crosslinking ability. To this aim, ALMA and DAAM were introduced in the amount of 1 wt.% concerning total monomer feeds, during the first and second step, and 5 wt.% with respect to the second step monomer feeds, respectively [44–46]. Details of the monomers composition and synthesis method are given in Supplementary Material (Table S1 and text above).

The solid content of the obtained polyacrylate latexes was about 33 wt.%. Dynamic light scattering measurements revealed the presence of nano-sized spherical polymer particles (with a diameter around 100 nm and low polydispersity, indicating insignificant agglomeration or secondary nucleation of polymer particles during polymerization process).

2.3 Preparation of the consolidated stone

Stone samples were cut as square parallele pipeds of the dimensions 4 × 4 × 25 mm^3. Before consolidation treatment, they have been washed and cleaned by sonication in water to remove residues from the shaping process. In a similar way to previous works [29,30], for Prague sandstone, three doses of latex dispersions, 12 µL each, were applied on one side of the dried specimens on three equally spaced points of the stone specimens using a micropipette, as schematically illustrated in Fig. 1, and left to penetrate by gravity. Owing to the finer pore network of the Oberkirchen sandstone of reduced permeability, an alternative application method (see Fig. 1), frequently documented in the literature [47], was adopted, that is, the specimens were soaked in the polymer dispersions for 30 seconds.

Three replicates for each stone treated with the 2 latex formulations were prepared. Conditioning was done at 25 °C and relative humidity of 60% for 7 days. The naming

convention adopted for the samples is XS_Y_Z, where X is P for the Prague and O for the Oberkirchen; S for sandstone; Y is A for the treatment with latex A and B for the treatment with latex B, and Z is the replicate number (from 1 to 3, when specification is needed).

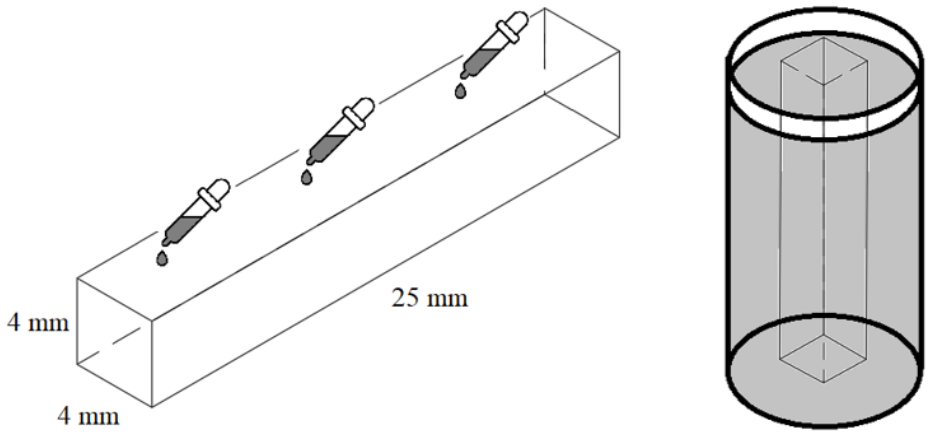

Fig. 1: Illustration of the methods of application of the consolidation agents in the case of samples composed of Prague sandstone (on the left) and Oberkirchen sandstone (on the right). The dimensions of samples have been identical in both treatment applications.

2.4 Analytical Methods

Conventional X-ray powder diffraction (XRPD) has been employed for the mineralogical characterization of the PS and OS. To this aim, powder diffraction patterns were collected on a LynxEye 1-D silicon strip detector in the angular range 5- 70º 2θ with a virtual step scan of 0.01º, counting 0.4 s per step adopting a D8 Advance Bragg-Brentano diffractometer (Bruker AXS). The Cu K_α radiation was selected with a Ni filter and generated at 40 kV and 40 mA and. In order to increase the particle statistics and reduce texture effects, the sample was allowed to spin at 15 rpm. Phase quantification was obtained by the Rietveld refinement of the XRPD data using the software Topas 4.2 (Bruker AXS).

The mCT data have been collected at the SYRMEP beamline of the Elettra synchrotron radiation facility (Trieste, Italy), employing a filter-hardened (1.0 mm Al + 1.5 mm Si) white

X-ray beam. The samples were mounted on a rotating stage and the mCT scans were recorded in the local area or region-of-interest mode [48] on an air-cooled 16-bit 2048 × 2048 pixels sCMOS camera (Hamamatsu C11440-22C), acquiring 1800 projections over a rotation of 180° with an exposure time/projection of 2.5 s. The effective pixel size was set to 1.95 × 1.95 μm working with the sample-to-detector distance of 150 mm. To improve the visibility of features with similar linear attenuation coefficients the propagation-based phase-contrast mode was adopted [33]. The SYRMEP Tomo Project software [49,50] was employed for tomographic reconstruction, adopting the Filtered Back Projection algorithm [51]. A single distance phase-retrieval algorithm was applied to enhance the contrast between the polymer and the pore space, thus, improving the reliability of quantitative image analysis. To this aim, the ratio $\gamma = \delta/\beta$ between the real and imaginary parts of the refractive index was set to 364 and 200 for the PS and OS samples, respectively.

The microstructure of the consolidated samples was also observed with a scanning electron microscope (SEM), after the mCT measurements. To this aim, cross-sections perpendicular to the direction of maximum elongation were obtained by cutting the specimens with a low-speed diamond saw without impregnation in epoxy to perturbe the microstructure the least. SEM observations were conducted on samples coated with a thin carbon film, to reduce charging effects, at 20 kV accelerating voltage using a backscatter electron detector mounted on a Quanta 450 FEG (FEI, Czech Republic) instrument.

Processing and analysis of SR-μCT images

The freeware software Fiji [52] was used for the visualization of the reconstructed or processed two-dimensional (2D) slices and the calculation of the porosity profile in depth within the samples.

Volumes of interest (VOIs) 2.34×2.34×3.32 mm^3, obtained from the reconstructed volumes, were adopted. For a better description of the polymer latex distribution within the stone pore network, they have been cropped as closest as possible to the surface of application of the polymer latex for the Prague sandstone and to one of the surfaces of the Oberkirchen sandstone samples (because of the penetration from all sides). Image segmentation was aimed at isolating the polymer from the stone matrix and pore network. To facilitate edge recognition, the anisotropic diffusion filter was applied before segmentation. Segmentation for Prague sandstone samples was accomplished by creating three regions of interest (ROIs) using the software Dragonfly (ORS Inc., Canada), one for each segmented volume (solid, pores and polymer). For the Oberkirchen sandstone samples, because of the difficulties in segmenting the polymer, only two ROIs were defined (solid + polymer and voids), again, using Dragonfly (ORS Inc., Canada) software. The impact of polymer on the pore network was obtained by subtraction of this ROI to the one (solid + voids) obtained from the samples measured before the treatment.

In all cases, the choice of grey level intervals was performed manually, in consideration of the low contrast difference between the polymer and the voids, and the distribution of the polymer, which was frequently concentrated on the pore walls, in form of a layer of variable thickness.

The ROIs were employed to perform quantitative image analysis. Total porosity (Φ (%)) was calculated in Dragonfly, pore surface area per unit volume of sample (S_V (mm^{-1})) and fractal dimension (D_F) were obtained with Pore3D software [53]; pore size distribution (PSD) and connectivity of the pore network were retrieved with Dragonfly, which was also employed for volume rendering procedures. Additionally, the pore network modelling method implemented in Dragonfly allowed for the extraction of water permeability and diffusion coefficient through the simulation of water transport properties.

3. Results and discussion

The mineralogical analysis of the stone samples, reported in Table 1 confirmed the large prevalence of quartz (> 96%) in both stones with a higher amount of quartz in the P sample and a higher presence of clay minerals in the O s, in substantial agreement with the literature [34,35,37].

Table 1: Quantitative phase analysis of the stones employed in the study. Standard deviations have been calculated to be less than 0.1.

Phase	**PS**	**OS**
	***c* / wt.%**	***c* / wt.%**
Quartz	97.4	96.3
Kaolinite	0.8	2.3
Illite/Muscovit	0.4	1.3
K-feldspar	1.4	-

3.1 Consolidation of Prague sandstone

Fig. 2 illustrates details of the microstructure of the Prague sandstone after the consolidation treatment, as observed in cross-section under SEM at different depths with respect to the surface of application. In two dimensional view (2D), the relatively large original porosity (mostly around 30 µm) possessing a good degree of connectivity, appeared to have been sensibly reduced by the presence of the consolidating agent. The latex consolidating agents exhibited a high pore-filling capacity as well as film-forming ability, covering the surface of the quartz grains of the stone matrix and bridging the grains (an example highlighted by inserted arrow in Fig. 2b). The polymer nanodispersions penetrated at high depth within the sample, and were detectable close to the opposite surface. The fluorinated and non-fluorinated polymers behaved apparently in a similar manner with respect to their distribution, adhesion and film-forming ability.

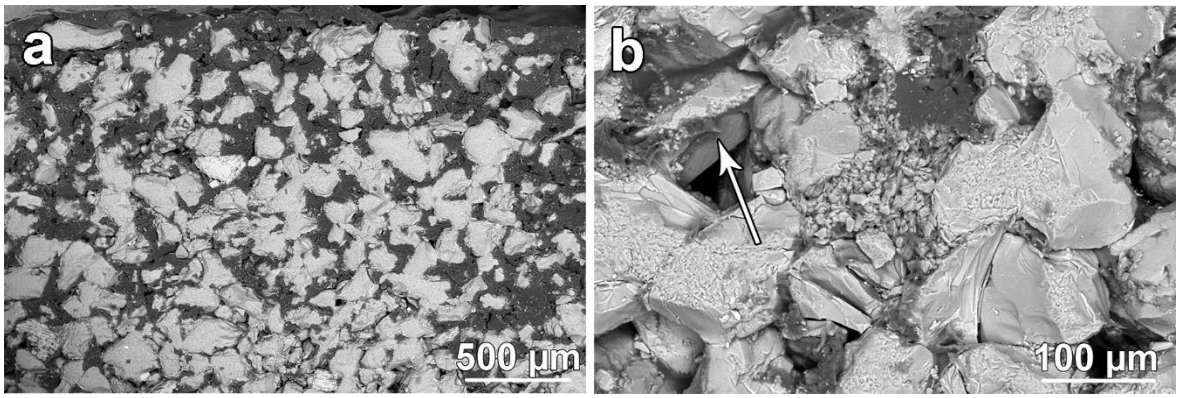

Fig. 2: SEM micrographs of the Prague sandstone samples after consolidation treatment. The surface of application is visible in the upper part of the Fig 2a. The arrow in Fig. 2b indicates an example of good ability of the polymer to bridging the grains.

When the investigation with mCT is considered, the preliminary steps for the extraction of accurate quantitative information from the investigated volumes, described in the experimental section, are schematically illustrated in Fig. 3. They were aimed at enhancing the separation in grey levels between the polymer and the voids, impaired by their small difference in contrast for X-rays.

Fig. 4 is an example of volume rendering illustrating the distribution of the latex polymer within the sample. From a qualitative standpoint, the polymer appeared to be more concentrated closer to the surface of application (upper part of the ROI), where the original voids were almost completely sealed.

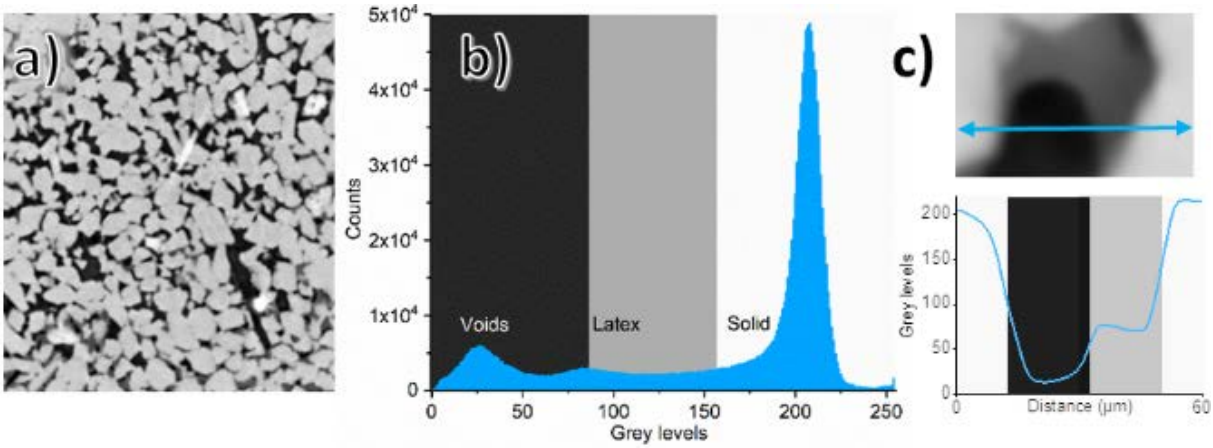

Fig. 3: An example of mCT axial view of the VOI (2.34×2.34×3.32 mm^3) in the reconstructed volume of the PS_A_01 sample after image filtering (a); histogram of grey levels with the thresholds adopted to extract the ROIs corresponding to the voids (1-75), latex (76-155) and solid (156-256) (b); distribution of grey levels along a line crossing the three source of contrast within the sample (c).

The high penetration ability observed with SEM was confirmed by mCT, since at the maximum distance from the surface of the application, the latex polymer could still be detected. The results of quantitative image analysis, as the average of the three sample replicates, are summarized in Table 2. The full data set is provided in Table S2 (Supplementary Material). When the total porosity of the untreated stone is considered, the values are within the range reported in the literature (26.3 – 29.7 vol.% [34]). The pore-filling effect of the latex is well evidenced by the significant decrease in porosity after the treatment, calculated between 7.0 and 7.6 %. The difference between the samples consolidated with latex A and B is within the standard deviation of the measurements, therefore, it might be attributed to the slightly different characteristics of the pore networks due to the natural variability of the stone. A similar concept holds for the specific surface S_V. In this case, for each sample replicate, S_V was always higher after the treatment, suggesting an increased complexity in the pore surface; the only exception was represented by the replicate PS_A_01

(see Table S2). This low value negatively impacted on the standard deviation of the average S_v reported in Table 2.

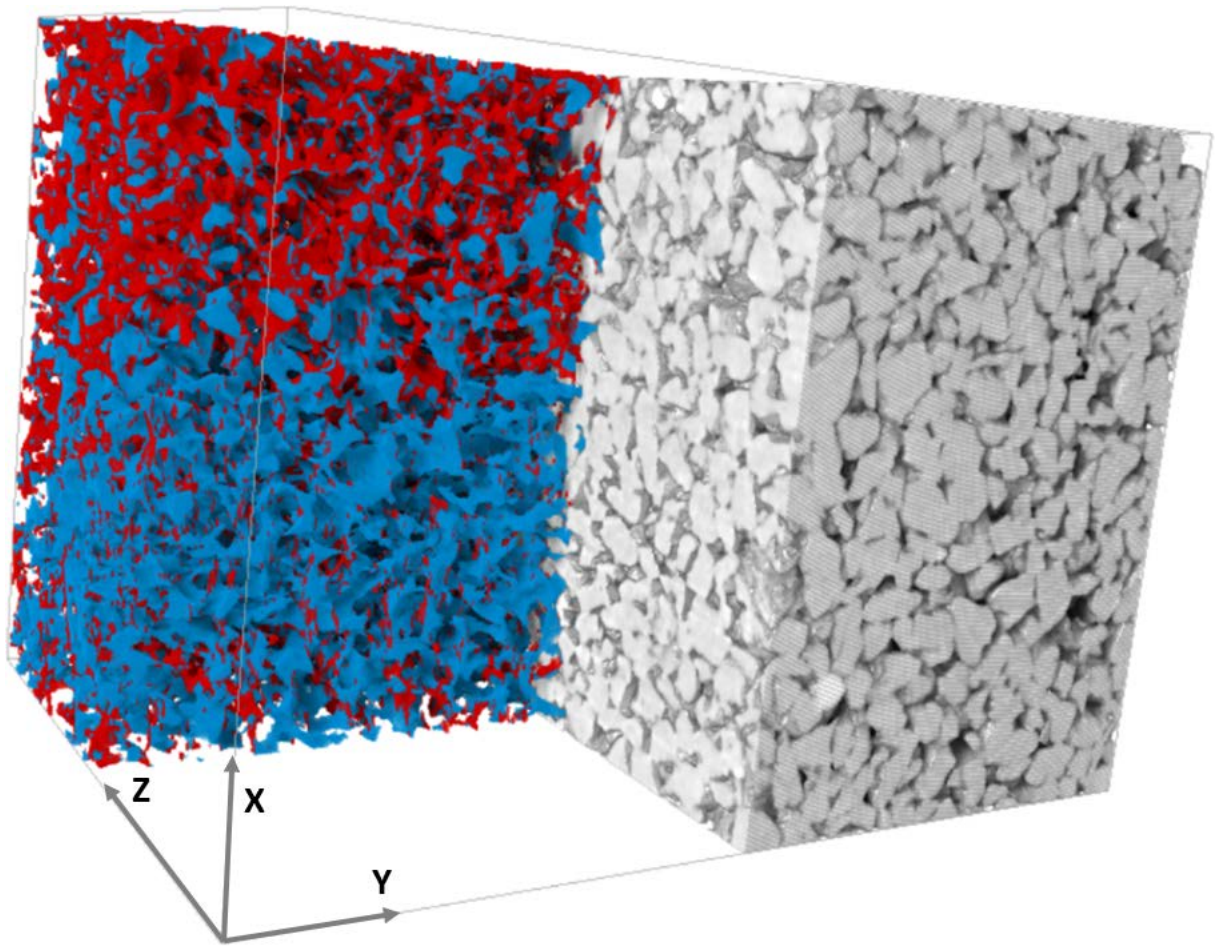

Fig. 4: 3D rendering of the studied volume of the PS_A_01 sample with a size of VOI 2.34 × 2.34 × 3.32 mm^3. A portion of the matrix has been removed to evidence the segmented voids (in blue) and the polymer distribution (in red). The surface of application of the consolidating agent was on top.

As for the fractal dimension, at the scale investigated by mCT, the polymer slightly reduced the 'roughness' of the pore surface, when such simplified interpretation of the D_F is accepted. The parameters of the pore size distribution obtained from the analysis of the VOIs (2.34×2.34×2.34 mm^3) are provided in Table S3. The mean of the PSD ranges between 23.4 – 23.7 µm and 18.8 – 21.0 µm in the samples before the treatment and after the treatment, respectively, with no significant difference between the two latex types.

Table 2: Results of quantitative image analysis (total porosity (Φ), pore surface area per unit volume of sample (S_V) and fractal dimension (D_F)) for the PS samples as the average of the three sample replicates (standard deviations are listed in brackets after last valid number).

Sample	Before treatment			After treatment			
	Φ (%)	S_V (mm^{-1})	D_F	Φ (%)	S_V (mm^{-1})	D_F	c_{Latex} (vol. %)
PS_A	27.1(5)	24.2(4)	2.67(1)	20(1)	25(2)	2.61(1)	7(1)
PS_B	26(2)	23.7(4)	2.66(1)	19(2)	25.3(6)	2.61(1)	8(1)

The reduction in the mean pore size is well illustrated by the shape of the PSD, as in the example reported in Fig. 5, related to the replicate PS_A_02. Most of the detected porosity spans the size range of 20−40 µm, but after the treatment, the total number of pores decreases and the shape of the distribution shifts towards lower values with a decrease in the number of larger pores.

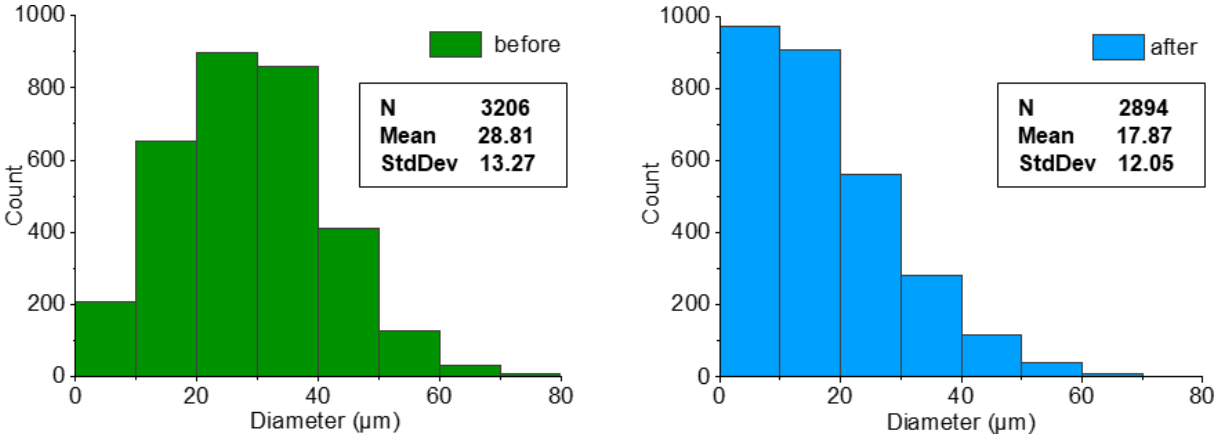

Fig. 5: Pore size distribution for PS_A_02 sample, as obtained from the analysis of the ROI before and after the treatment, isolated pores included. The total number of voids (N), mean and standard deviation of the distribution are indicated.

The impact of the treatment on the structure of the pore network can be evaluated also through pore connectivity. The parameters obtained from the connectivity analysis for each sample replicate are provided in Table S4. The mean pore connectivity ranged between 4.18 and 4.39 in the sample without polymer, and decreased to 2.7 – 3.1 in the treated samples, again with no significant differences between the latex types. Fig. 6 illustrates an example of a histogram of pore connectivity for the same sample as in Fig. 4 (PS_A_01). In this case, the distribution has been found to be sharpened and peaked at lower connectivity values after the treatment, whereas the frequency increased. A remarkable increase in the number of isolated pores (with zero connectivity) occurred, reflecting the ‘sealing’ effect of the polymer.

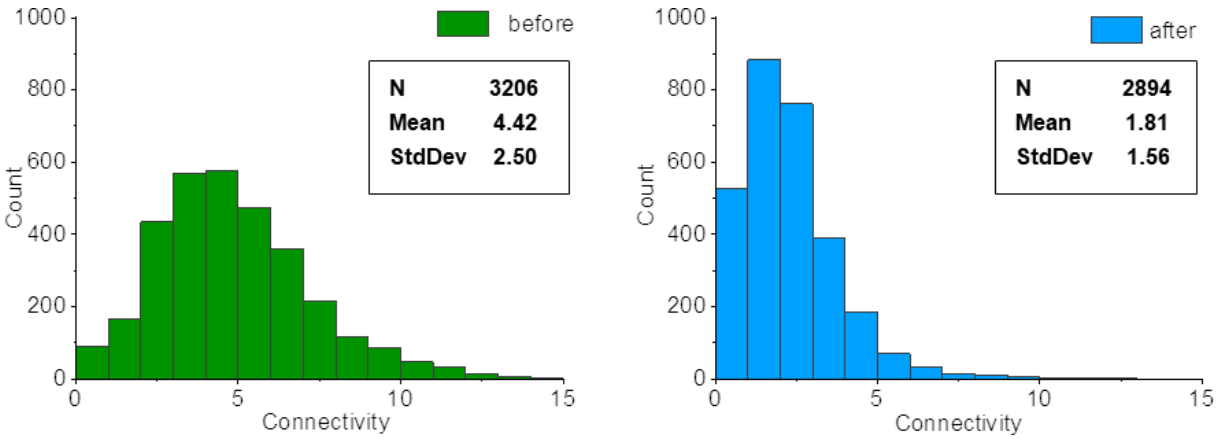

Fig. 6: Pore connectivity histogram for PS_A_02, as obtained from the analysis of the VOI, isolated pores included. The total number of voids (N), mean and standard deviation of the distribution, are indicated.

Owing to the method of application of the consolidating agent, a strongly asymmetric distribution of the porosity within the sample should be expected. Accordingly, Fig. 7a shows that the porosity calculated from mCT slices cut parallel to the surface of application at increasing distance from the surface, increases steadily in the untreated sample, so that the difference between the two models (before and after the treatment) decreases up to a distance corresponding, more or less, to the centre of the VOI (slice 600, corresponding to 1170 μm). This trend is less marked afterwards. The minimum difference measured in the centre of the VOI was found to be 4%. Such trend indicates that the pore-filling effect of the consolidating treatment should be relevant up to a distance of about 1.5 mm (considering that the VOI was cut at some distance from the sample surface), but it still presents afterwards, as suggested by the qualitative analysis of mCT segmented volumes (Fig. 4) and by direct observation under SEM. The impact of the treatment is also illustrated through the simplified graphical representation of the pore network in Fig. 7b.

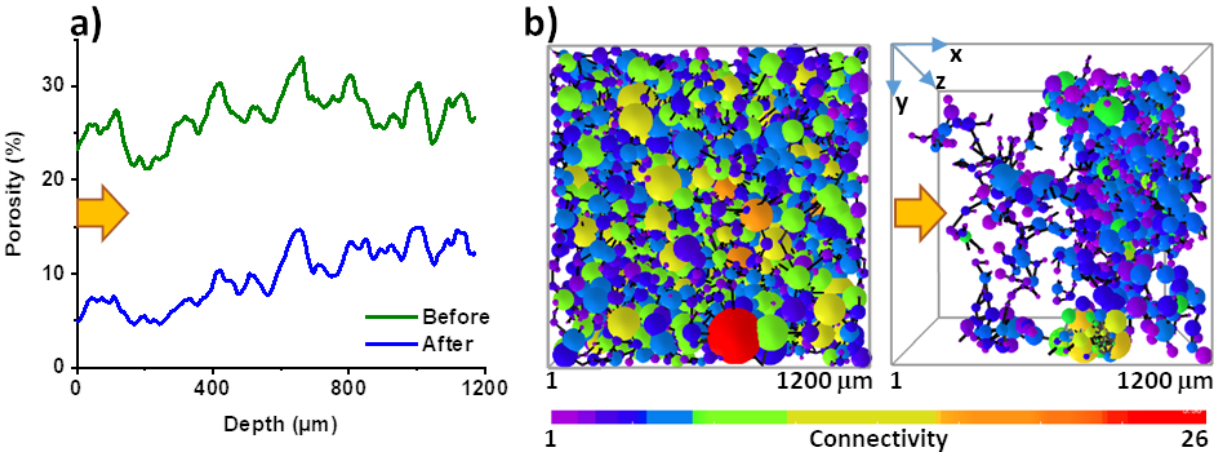

Fig. 7: Plot of the porosity calculated from slices parallel to the surface of application of the consolidating agent at increasing depth within the sample PS_A_02 (a). Simplified representation of the pore network on the VOI selected for the analysis (1.17×1.17×1.17 mm^3). The state of the sample before and after the treatment is illustrated in Fig. 7a and Fig. 7b, respectively. The direction of penetration of latex, according to the surface of the application, is indicated by an arrow.

The parameters of water transport within the sample volume, obtained from the pore network modelling tool, sheds further light on the protective action of the polymer against weathering effects. Obtained values of tensors representing the water permeability (Fig. 8) and diffusion coefficient are provided for all sample replicates in Tables S5-6. In the stone before treatment, both permeability and diffusion coefficients resulted lower along the x direction. Upon application of the polymer consolidating agent, an impressive decrease of more than one order of magnitude was obtained in both parameters. The effect was enhanced along the x direction. This increased anisotropy is the effect of the penetration of the latex from the surface, which occurred along the x direction. It should be noted that, the differences between the sample replicates, measured after the treatment, are high in reason of the

distribution of the polymer within the pore network, which induced high variability in the pore connectivity.

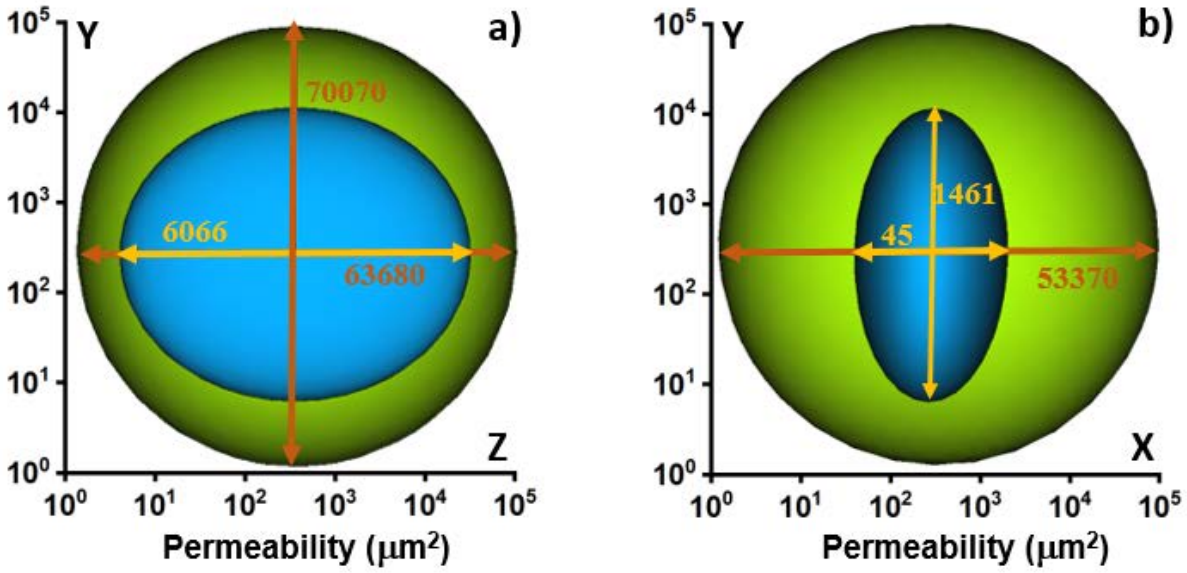

Fig. 8: Visualization of permeability tensors in a logarithmic scale (log_{10}); two different views (a) and (b) are 90° apart. Permeability tensors of PS_B_02 sample before the latex application are visualized in green; permeability tensors after the treatment are visualized in blue.

3.2 Oberkirchen sandstone

The microstructure of the Oberkirchen sandstone, observed in the cross-section under SEM, is illustrated in Fig. 9. The difference from the PS samples is apparent (Fig. 2). In the case of the OS samples, both the average size of pores and the penetration of the consolidating agent within the sample volume were higher. Notably, a fraction of small particles, most likely phyllosilicates or clay minerals (indicated by arrows in Fig. 9b), were observed between the quartz grains which comprise the large majority of the solid matrix. This is in agreement with the presence of kaolinite and illite/muscovite detected with XRPD

(Table 1). As observed for the PS samples, also in OS samples no difference between fluorinated and non-fluorinated polymers was not noticeable in the distribution of the polymer and its adhesion to the grain surface.

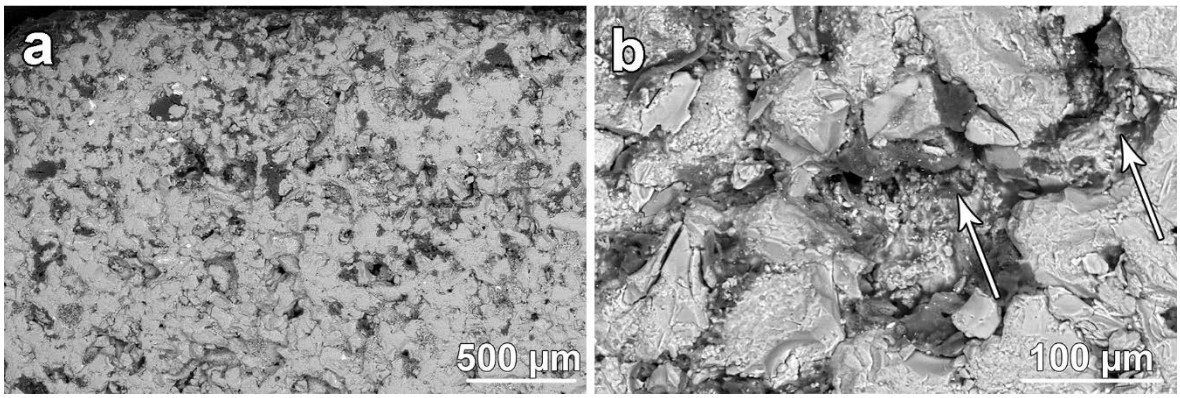

Figure 9: SEM micrographs of the Oberkirchen sandstone samples after consolidation treatment. The surface of the application is visible in the upper part in the Fig. 9a. The presence of phyllosilicates and clay minerals is highlighted by arrows in Fig. 9b.

The lower contrast for X-rays of the phyllosilicates, more similar to the consolidating agent, with respect to the quartz grains, impaired the accuracy of the segmentation of the polymer during the analysis of the mCT images (see Fig. 10). The procedure was also complicated by the finer microstructure and lower total porosity compared to the Prague sandstone. Examples of grey levels distributions in both stones are reported in Fig. S1, whereas attempts to perform segmentation on the samples after the treatment are illustrated in Fig. S2. As mentioned earlier in section 2.4, to improve the accuracy of the quantitative image analysis, for OS samples the analysis was conducted separately on the same sample volumes collected before and after the consolidation treatment.

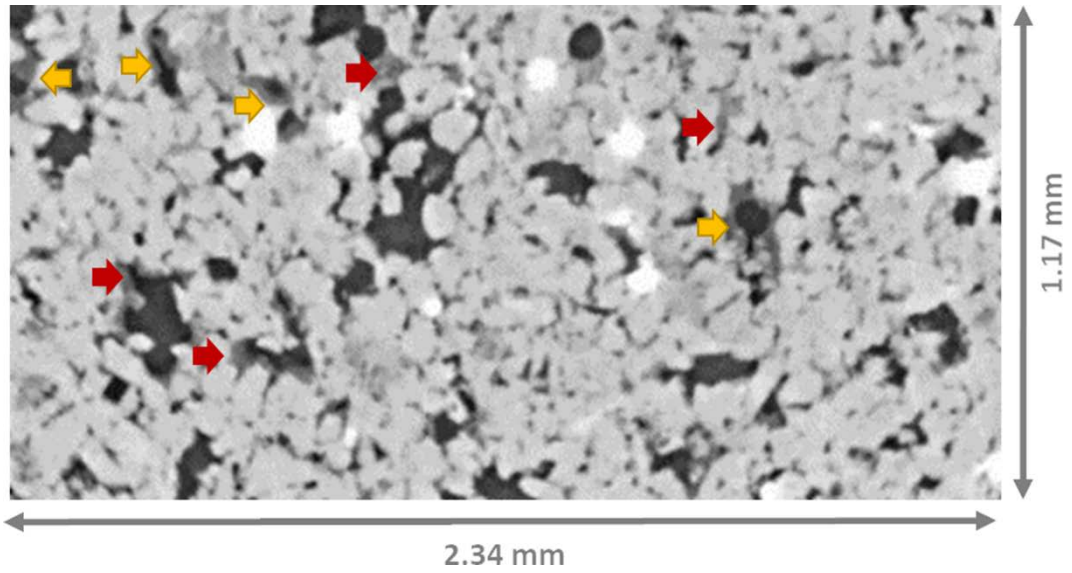

Fig. 10: mCT axial view of the VOI in the reconstructed volume of one of the OS samples after the latex application, image filtered. Examples of the latex in the matrix, as detected by comparison with the untreated sample, are indicated by yellow arrows. The red arrows highlight some places where the stone matrix exhibits a similar distribution of grey levels as the latex.

As shown in Fig. 11, the amount of polymer which penetrated into the pore volume (in red in the figure) is much less compared to the sample PS (see Fig. 4), but the consolidating agent appears more homogeneously distributed in depth. A slightly higher concentration is observed in the upper part because this side of the VOI was the one closer to the external surface of the specimen.

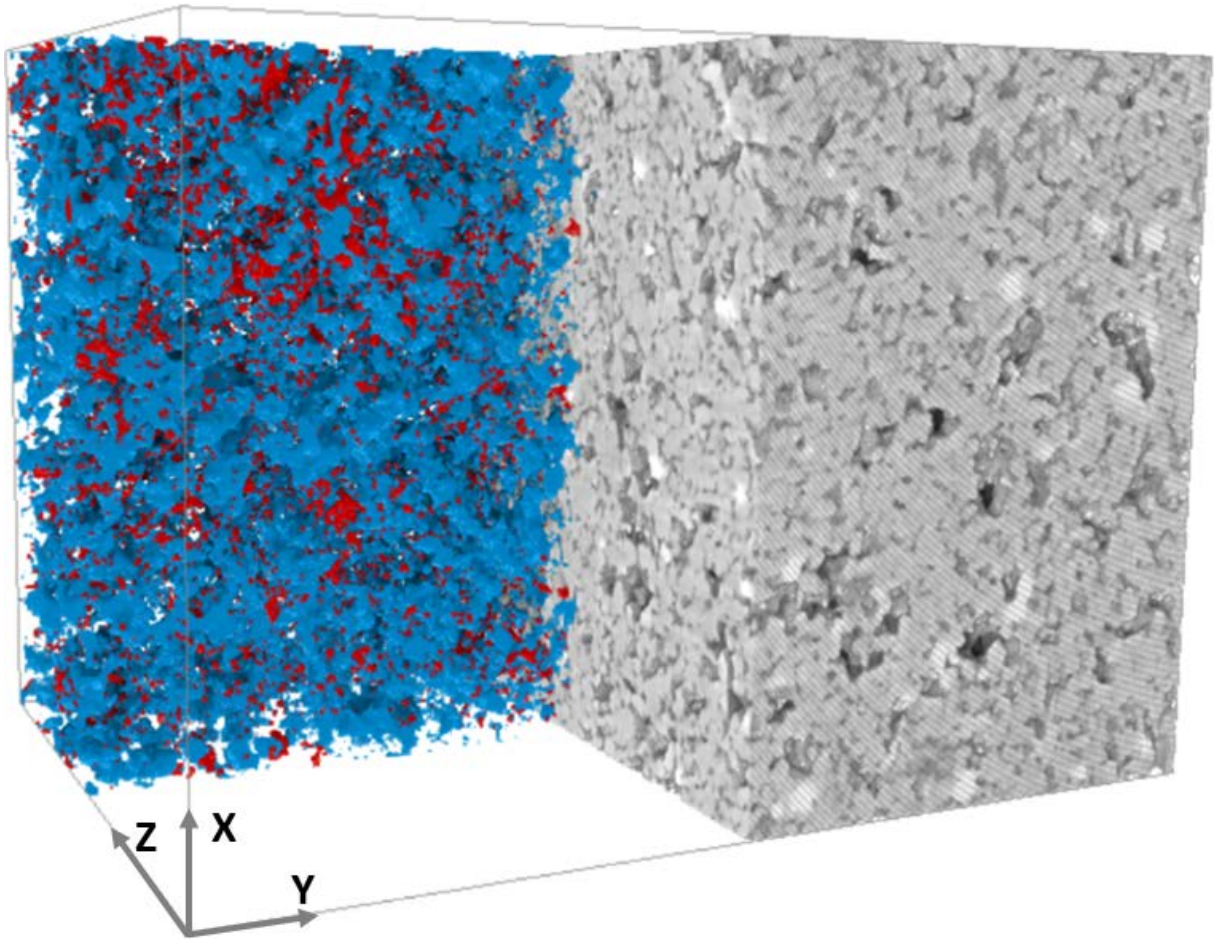

Fig. 11: The 3D rendering of the VOI 2.34×2.34×3.32 mm^3 from the sample OS_A_01. The matrix has been partly removed to highlight the distribution of the polymer (in red) and remaining voids (in blue).

Table 4 reports the results of quantitative image analysis as the average of the three sample replicates. The whole dataset is provided in Table S7. The much lower porosity with respect to the PS samples explains the lower depth of penetration observed with microscopy and in the mCT axial views. The absolute values of porosity are slightly lower than most of the data from the literature. This could be due to a systematic error originated by the segmentation procedure, but it could be also explained by the natural variability of the stone,

as confirmed by the wide range of values reported in the literature [37,38]. All in all, the effect of the treatment on the porosity measured in the VOIs has been quantified to be below 2.5% in volume. Also, for the OS samples, the two polymers exhibited the same pore-filling behaviour.

Table 4: Results of quantitative image analysis (total porosity (Φ), pore surface area per unit volume of sample (S_V) and fractal dimension (D_F)) for the OS samples as the average of the three sample replicates (standard deviations are listed in brackets after last valid number).

Sample	Before treatment			After treatment			
	Φ (%)	S_V (mm^{-1})	D_F	Φ (%)	S_V (mm^{-1})	D_F	c_{Latex} (vol.%)
OS_A	12.6(2)	15.6(6)	2.51(1)	10(1)	14(1)	2.47(3)	2(1)
OS_B	12.9(4)	15.8(3)	2.52(1)	10.8(2)	14.2(4)	2.49(1)	2.1(3)

Unlike the PS samples, the specific surface of the pores resulted systematically lower after the treatment. Accordingly, the complexity of the pore surface decreased after the treatment, as suggested by the slightly lower fractal dimension D_F. This pinpoints the completely different effect that the same consolidating agents may have on different stones in reason of their different microstructure.

An example of the pore size distribution, obtained from the analysis of the VOI (1.17 × 1.17 × 1.17 mm^3), is graphically illustrated in Fig. 12; the complete data set is provided in Table S8.

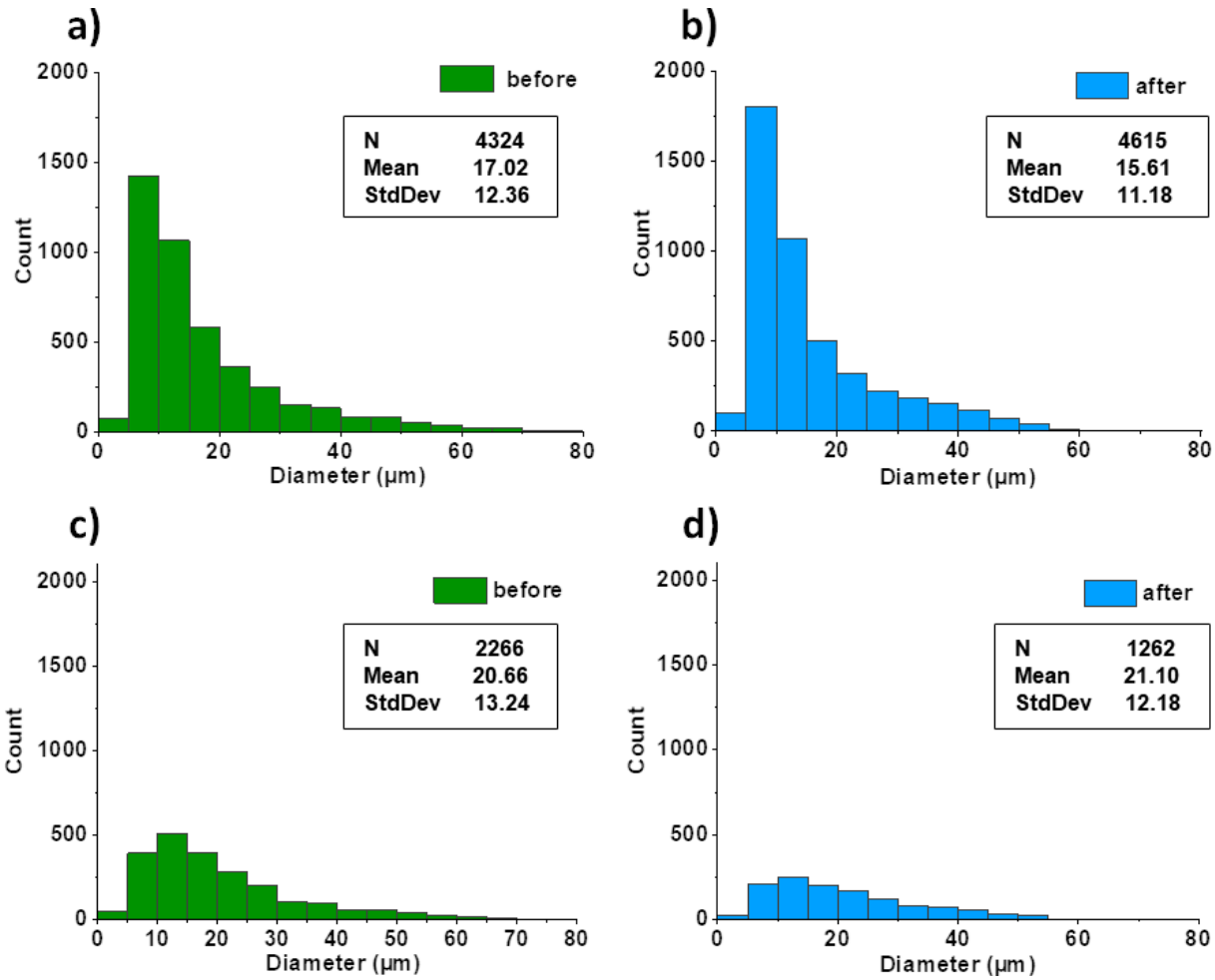

Fig. 12: Pore size distribution for the sample OS_B_03; isolated pores included (a, b) and isolated pores excluded (c,d). Total number of voids (N), mean and standard deviation of the distribution, are indicated

The mean values of the PSD in the samples before and after the treatment substantially overlap, ranging between 18.0 and 21.5 µm, with no significant difference between the two latex types. When the total porosity is considered (Fig. 12a-b), after the treatment the number of pores (open + closed) increases, the distribution become sharper (lower standard deviation) and shifts towards finer pore sizes (lower mean).

There is clear evidence that the increase in the number of pores after the treatment resulted from the partial obstruction of larger pores, with the creation of more, smaller ones.

This explains the higher number of pores with equivalent diameters between 5 and 10 µm and the lower number of pores with equivalent diameters > 20 µm, those most affected by the presence of latex. This view is corroborated by the analysis conducted by excluding the isolated pores (Fig. 12c-d), which evidenced a marked overall decrease in the number of open pores.

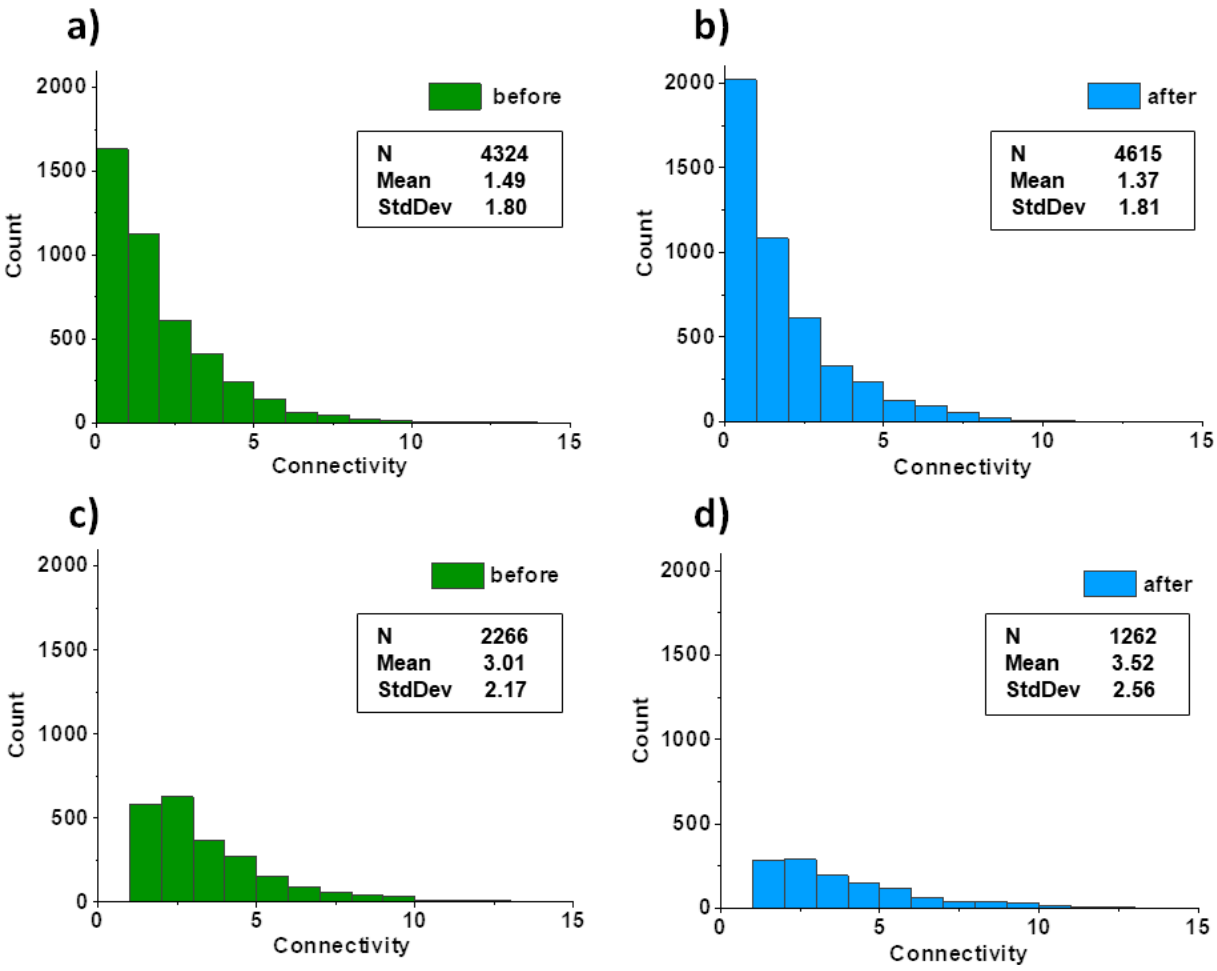

Fig. 13: Pore connectivity histogram for the sample OS_B_03, as obtained from the analysis of the VOI (1.17 × 1.17 × 1.17 mm^3), isolated pores included (a-b) and isolated pores excluded (c-d). Total number of voids (N), mean and standard deviation of the distributions, are indicated.

The impact of the treatment on the structure of the pore network can be evaluated also through the changes in pore connectivity. The results of the analysis for each sample replicate are provided in Table S9. Fig. 13 illustrates an example of a histogram of pore connectivity for the same sample as in Fig. 12. The mean pore connectivity was calculated from the model with and without isolated pores. As a general remark, compared to the samples PS (Fig. 6), the pore network of samples OS exhibits lower connectivity and a more asymmetric distribution. Nonetheless, a similar effect was observed after the treatment, that is, the distribution sharpened towards lower connectivity values, whereas the frequency increased for the lowest connectivity, with no significant differences concerning the latex type. This increase in the number of isolated pores reflected the effective 'sealing' effect of the polymer.

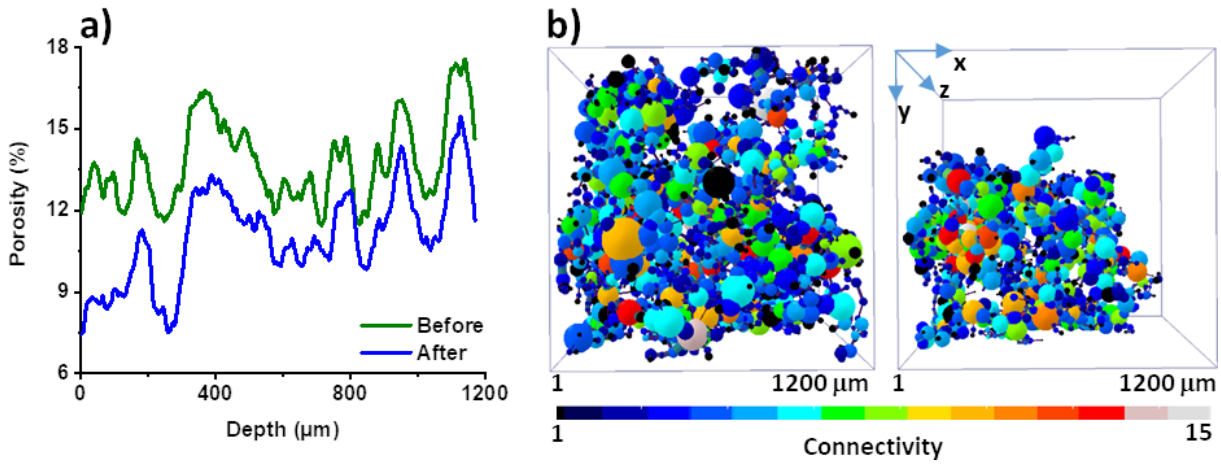

Fig. 14: Plot of the porosity calculated for the VOI (1.17 × 1.17 × 1.17 mm^3) from slices at increasing depth within the sample OS_B_03 (a). Simplified representation of the pore network on the same sample before and after the treatment (b). The +x direction is from the closest surface of the specimen to the centre of the sample.

Fig. 14a shows an example of the porosity calculated for slices at increasing distance from one of the faces of the VOI, located close to the external surface of the specimen. The curve of the treated sample is approaching the one of the untreated samples, and after 0.5 mm the difference in porosity is between 1.5 and 2.0%. This small, but detectable difference indicates that the polymer is penetrating in depth within the sample, as observed in the volume rendering shown in Fig. 11. The graphical representation of the pore network before and after the treatment, illustrated in Fig. 14b, further confirmed the void-sealing effect of the polymer, which, unlike the PS samples (Fig. 7), developed from all directions, because of the different application method of the consolidating agent.

Results of simulation of water transport properties within the samples are provided for all sample replicates in Table S10. For some of the sample replicates, the calculation of water permeability could not be completed due to hardware and software limitations. This was certainly due to the much finer microstructure of the OS, compared to the PS. For the same reasons, diffusivity values could not be calculated in case of OS samples. The obtained values of permeability showed that, in the untreated stone, permeability values were more than one order of magnitude lower with respect to the PS samples. Nonetheless, the values were scattered and so were the components of the tensor. This dispersion of the anisotropy, likely related to the method of application of the consolidating agent (from all directions towards the centre of the specimen), no unequivocal modification of the shape of the ellipsoids could be observed. In the example of sample OS_A_02, shown in Fig. 15, in the untreated stone permeability is nearly isotropic (nearly spherical green shape), whereas, after the treatment, a significant decrease can be observed in the x-z plane (blue shapes).

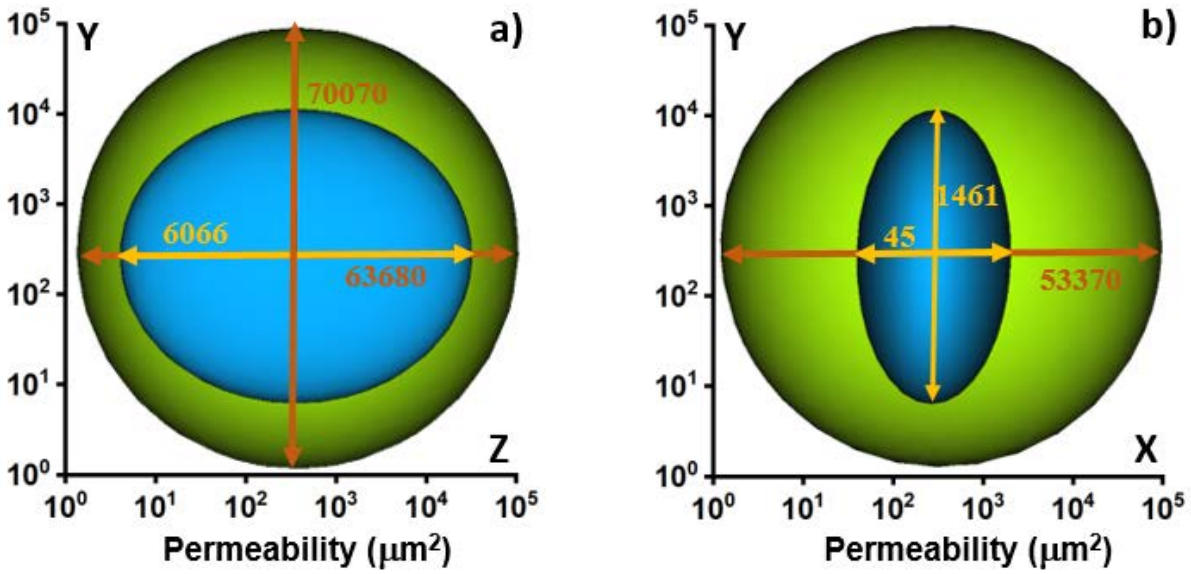

Fig. 15: Visualization of permeability tensors in a logarithmic scale (log_{10}); two different views (a) and (b) are 90° apart. Permeability tensor of PS_B_02 sample before the latex application is visualized in green; permeability tensor after the treatment is visualized in blue.

The presented results indicated that both the synthesized acrylic latexes possessed a good pore-filling ability in the two types of sandstone studied. As expected, the extent of this effect is strongly dependent on the characteristics of the pore network, which explains the decrease of > 7% for the PS samples with initial porosity > 25% and 2.0-2.5% for the OS samples with initial porosity in the range from 16 to 20%. Consequently, for PS the penetration depth exceeded the sample thickness (4 mm) and for the OS was mainly limited to the first 0.5 mm. Nonetheless, significant effects were observed when fluid transport properties were considered, since the simulations evidenced a decrease in permeability and diffusion coefficient of more than one order of magnitude. This decrease is strongly anisotropic, occurring essentially along the direction of latex penetration.

Concerning the measured properties, both the fluorinated and non-fluorinated polymers behaved similarly with respect to their spatial distribution, adhesion and film-

forming ability. Therefore, the main difference between the two materials is in their hydrophobicity. This characteristic is expected to impact on other properties, like improved resistance against weathering. Such investigation falls outside the aim of the present work and will be the object of a future study.

In terms of physical-chemical interactions, it can be observed that, on one side, the negatively charged acrylic latex particles are expected to be facilitated in their penetration within the sandstone pore network thanks to the electrostatic repulsion with the negatively charged quartz particles (the point of zero charge of quartz is ~ 2 [54]), and, on the other side, the good film forming ability of latex impairs water penetration and enhances stone cohesion. The latter aspect is of great interest in stone conservation; notably, as recently observed in organic-inorganic cement composites, along with the improvement in mechanical performance, latex is expected to impart ductility to an otherwise brittle material [55]. This increased ability to deform under stress is observed also after failure, so that the material may accommodate large deformation while preserving some residual strength sensibly postponing the collapse of the object.

The quantitative information on the effect of the consolidation treatment gathered in this study has not an equivalent in the literature. Available results based on mCT are essentially qualitative descriptions of the changes induced by the treatment [32], or a mere evaluation of penetration depths [26,31]. In our previous works [29,30], quantitative parameters, *e.g.* porosity, surface per unit volume (S_V) and fractal dimension (D_F), have been obtained for the Maastricht limestone treated with nanolime or nanolime in combination with different calcium carbonate polymorphs. The detected changes in porosity were found to be sensibly lower compared with the data presented above, although the consolidation agents were at lower concentration. No significant differences were found in the values of S_V whereas, D_F has been found to be higher after the treatment, indicating an increase in

microstructural complexity and/or surface roughness. Such differences can be ascribed to the different nature of the consolidation agent but also to the different characteristics of the stone microstructure and pore network.

It is worth noting that the mCT technique allowed for the extraction of a high amount of quantitative data in a fully non-invasive fashion, demonstrating its high potential for the characterization of the treatments and the prediction of their effectiveness. It has been shown that this can be done when the separation of the polymer from the voids is possible. In more complex systems, this possibility is not completely precluded but it requires the measurement of the samples before and after the treatment, as for the case of O sandstone described in this work.

4 Conclusions

Two representatives of porous sandstones, Prague (Mšené) and Oberkirchen, used in the past to build important objects of our Cultural Heritage have been selected to investigate the effectiveness of consolidation treatment using innovative laboratory-synthetized aqueous polyacrylate latex nanosuspensions, with and without fluorination, using synchrotron micro-computed tomography. Several quantitative parameters have been extracted in a fully non-invasive fashion adopting tools for image analysis and advanced modelling of water penetration has been accomplished. Both latexes exhibited similar film-forming ability and pore-filling ability. The effect of the treatment was different between the two stones in reason of the different characteristics of their pore network.

In the case of the Prague sandstone, the total porosity of treated samples has been calculated to be lower by around 7%, a number in good agreement with the obtained volumetric concentration of intruded latex nanoparticles. Such a high reduction in porosity was in agreement with the decrease in the number of voids, their mean size as well as the shift

of pore connectivity to lower values. Pore surface per unit volume has been identified to be slightly higher after the treatment suggesting increased microstructural complexity. The modelling of water permeability and diffusivity has resulted in tremendous, even one order of magnitude, decrease in both parameters mostly observed along the direction of penetration of the consolidating agent.

The Oberkirchen sandstones exhibited a decrease of total porosity of about 3% as a result of its finer and less connected microstructure. Opposite to Prague sandstone, pore surface per unit volume has been calculated to be slightly lower suggesting a decrease in microstructural complexity. Due to the presence of a high number of isolated pores, the clear changes in pore size distribution and pore connectivity have been revealed only after their exclusion. A decrease in water permeability and diffusivity was also observed, however, the change in shape of the corresponding ellipsoids was less clear, because of the different application procedure of the consolidation agents. Overall, mCT was successfully applied to derive quantitative information about the effectiveness of the consolidation treatment in a fully non-invasive fashion.

Acknowledgements

This research was funded by the Czech Academy of Sciences, Institute of Theoretical and Applied Mechanics - RVO 68378297. + others grants? We thank doc. Ing. Zuzana Slížková, Ph.D. and Dr. rer. nat. Matea Urbanek for the supply of Prague sandstone and Oberkirchen sandstone, respectively.

References

[1] S. Siegesmund, R. Snethlage, eds., Stone in Architecture, Springer Berlin Heidelberg, Berlin, Heidelberg, 2011. https://doi.org/10.1007/978-3-642-14475-2.

[2] R. Striani, C. Esposito Corcione, G. Dell'Anna Muia, M. Frigione, Durability of a sunlight-curable organic–inorganic hybrid protective coating for porous stones in natural and artificial weathering conditions, Prog. Org. Coatings. 101 (2016) 1–14. https://doi.org/10.1016/j.porgcoat.2016.07.018.

[3] A.P. Ferreira Pinto, J. Delgado Rodrigues, Consolidation of carbonate stones: Influence of treatment procedures on the strengthening action of consolidants, J. Cult. Herit. 13 (2012) 154–166. https://doi.org/10.1016/j.culher.2011.07.003.

[4] R. van Hees, R. Veiga, Z. Slížková, Consolidation of renders and plasters, Mater. Struct. Constr. 50 (2017) 1–16. https://doi.org/10.1617/s11527-016-0894-5.

[5] F. Xu, D. Li, Effect of the addition of hydroxyl-terminated polydimethylsiloxane to TEOS-based stone protective materials, J. Sol-Gel Sci. Technol. 65 (2013) 212–219. https://doi.org/10.1007/s10971-012-2926-0.

[6] M.L. Tabasso, Acrylic Polymers for the Conservation of Stone: Advantages and Drawbacks, APT Bull. 26 (1995) 17. https://doi.org/10.2307/1504445.

[7] E. Doehne, C.A. Price, Stone conservation: An overview of current research, Los Angeles, 2010.

[8] Y. Cao, A. Salvini, M. Camaiti, Oligoamide grafted with perfluoropolyether blocks: A potential protective coating for stone materials, Prog. Org. Coatings. 111 (2017) 164–174. https://doi.org/10.1016/j.porgcoat.2017.05.010.

[9] H. Zhang, Q. Liu, T. Liu, B. Zhang, The preservation damage of hydrophobic polymer

coating materials in conservation of stone relics, Prog. Org. Coatings. 76 (2013) 1127–1134. https://doi.org/10.1016/j.porgcoat.2013.03.018.

[10] I. Karapanagiotis, A. Pavlou, P.N. Manoudis, K.E. Aifantis, Water repellent ORMOSIL films for the protection of stone and other materials, Mater. Lett. 131 (2014) 276–279. https://doi.org/10.1016/j.matlet.2014.05.163.

[11] M. Licchelli, M. Malagodi, M.L. Weththimuni, C. Zanchi, Water-repellent properties of fluoroelastomers on a very porous stone: Effect of the application procedure, Prog. Org. Coatings. 76 (2013) 495–503. https://doi.org/10.1016/j.porgcoat.2012.11.005.

[12] M. Favaro, R. Mendichi, F. Ossola, S. Simon, P. Tomasin, P.A. Vigato, Evaluation of polymers for conservation treatments of outdoor exposed stone monuments. Part II: Photo-oxidative and salt-induced weathering of acrylic-silicone mixtures, Polym. Degrad. Stab. 92 (2007) 335–351. https://doi.org/10.1016/j.polymdegradstab.2006.12.008.

[13] A.E. Charola, Water-Repellent Treatments for Building Stones: A Practical Overview, APT Bull. 26 (1995) 10. https://doi.org/10.2307/1504480.

[14] W. Chen, C.J. Xiao, Z.J. Xu, X.N. Jiang, K.F. Zhou, A.P. Zhu, Q. Li, New water-based anti-corrosion chemical materials in engineering Repairing, in: Adv. Mater. Res., Trans Tech Publ, 2011: pp. 249–252.

[15] M.L. Picchio, M.C.G. Passeggi Jr, M.J. Barandiaran, L.M. Gugliotta, R.J. Minari, Waterborne acrylic–casein latexes as eco-friendly binders for coatings, Prog. Org. Coatings. 88 (2015) 8–16.

[16] D. Steinerová, A. Kalendová, J. Machotová, M. Pejchalová, Environmentally Friendly Water-Based Self-Crosslinking Acrylate Dispersion Containing Magnesium

Nanoparticles and Their Films Exhibiting Antimicrobial Properties, Coatings. 10 (2020) 340. https://doi.org/10.3390/coatings10040340.

[17] M. Mazzola, P. Frediani, S. Bracci, A. Salvini, New strategies for the synthesis of partially fluorinated acrylic polymers as possible materials for the protection of stone monuments, Eur. Polym. J. 39 (2003) 1995–2003. https://doi.org/10.1016/S0014-3057(03)00110-1.

[18] G. Alessandrini, L. Toniolo, C. Colombo, Partially fluorinated acrylic copolymers as coatings for calcareous stone materials, Stud. Conserv. 45 (2000) 1–6. https://doi.org/10.1179/sic.2000.45.supplement-1.1.

[19] H. Ling, L. Junyan, Synthesis, modification and characterization of core-shell fluoroacrylate copolymer latexes, J. Fluor. Chem. 129 (2008) 590–597. https://doi.org/10.1016/j.jfluchem.2008.04.007.

[20] W. Xu, Q. An, L. Hao, L. Huang, Synthesis, film morphology, and performance of cationic fluorinated polyacrylate emulsion with core-shell structure, J. Appl. Polym. Sci. 125 (2012) 2376–2383. https://doi.org/10.1002/app.36477.

[21] Q. An, W. Xu, L. Hao, L. Huang, Cationic fluorinated polyacrylate core-shell latex with pendant long chain alkyl: Synthesis, film morphology, and its performance on cotton substrates, J. Appl. Polym. Sci. 127 (2013) 1519–1526. https://doi.org/10.1002/app.37553.

[22] J.W. Ha, I.J. Park, S.B. Lee, D.K. Kim, Preparation and characterization of core-shell particles containing perfluoroalkyl acrylate in the shell, Macromolecules. 35 (2002) 6811–6818. https://doi.org/10.1021/ma011692u.

[23] G. Xu, L. Deng, X. Wen, P. Pi, D. Zheng, J. Cheng, Z. Yang, Synthesis and

characterization of fluorine-containing poly-styrene-acrylate latex with core–shell structure using a reactive surfactant, J. Coatings Technol. Res. 8 (2011) 401–407.

[24] J. Machotová, E. Černošková, J. Honzíček, J. Šňupárek, Water sensitivity of fluorine-containing polyacrylate latex coatings: Effects of crosslinking and ambient drying conditions, Prog. Org. Coatings. 120 (2018) 266–273. https://doi.org/10.1016/j.porgcoat.2018.03.016.

[25] J. Machotová, A. Kalendová, D. Steinerová, P. Mácová, S. Šlang, J. Šňupárek, J. Vajdák, Water-resistant latex coatings: Tuning of properties by polymerizable surfactant, covalent crosslinking and nanostructured zno additive, Coatings. 11 (2021) 347. https://doi.org/10.3390/coatings11030347.

[26] K. Niedoba, Z. Slížková, D. Frankeová, C.L. Nunes, I. Jandejsek, Modifying the consolidation depth of nanolime on Maastricht limestone, Constr. Build. Mater. 133 (2017) 51–56.

[27] V. Cnudde, J.P. Cnudde, C. Dupuis, P.J.S. Jacobs, X-ray micro-CT used for the localization of water repellents and consolidants inside natural building stones, Mater. Charact. 53 (2004) 259–271. https://doi.org/10.1016/j.matchar.2004.08.011.

[28] A. Brunetti, S. Bidali, A. Mariani, R. Cesareo, X-ray tomography for the visualization of monomer and polymer filling inside wood and stone, in: U. Bonse (Ed.), 2004: p. 191. https://doi.org/10.1117/12.560030.

[29] R. Ševčík, A. Viani, L. Mancini, M.-S. Appavou, D. Machová, Investigation of nano-microstructural changes in Maastricht limestone after treatment with nanolime suspension, Appl. Phys. A. 126 (2020) 367. https://doi.org/10.1007/s00339-020-03567-6.

[30] R. Ševčík, A. Viani, D. Machová, G. Lanzafame, L. Mancini, M.S. Appavou, Synthetic calcium carbonate improves the effectiveness of treatments with nanolime to contrast decay in highly porous limestone, Sci. Rep. 9 (2019). https://doi.org/10.1038/s41598-019-51836-z.

[31] M. Slavíková, F. Krejčí, J. Žemlička, M. Pech, P. Kotlík, J. Jakůbek, X-ray radiography and tomography for monitoring the penetration depth of consolidants in Opuka – the building stone of Prague monuments, J. Cult. Herit. 13 (2012) 357–364. https://doi.org/10.1016/j.culher.2012.01.010.

[32] V. Cnudde, P. Dubruel, K. De Winne, I. De Witte, B. Masschaele, P. Jacobs, E. Schacht, The use of X-ray tomography in the study of water repellents and consolidants, Eng. Geol. 103 (2009) 84–92. https://doi.org/10.1016/j.enggeo.2008.06.013.

[33] S.W. Wilkins, T.E. Gureyev, D.C. Gao, A. Pogany, A.W. Stevenson, Phase-contrast imaging using polychromatic hard X-rays, Nature. 384 (1996) 335–338. https://doi.org/10.1038/384335a0.

[34] V. Rybařík, Ušlechtilé stavební a sochařské kameny České republiky, Nadace Střední průmyslové školy kamenické a sochařské, 1994.

[35] Z. Pavlík, P. Michálek, M. Pavlíková, I. Kopecká, I. Maxová, R. Černý, Water and salt transport and storage properties of Mšené sandstone, Constr. Build. Mater. 22 (2008) 1736–1748. https://doi.org/10.1016/j.conbuildmat.2007.05.010.

[36] M. Remzova, R. Zouzelka, J. Lukes, J. Rathousky, Potential of Advanced Consolidants for the Application on Sandstone, Appl. Sci. 9 (2019) 5252. https://doi.org/10.3390/app9235252.

[37] C.W. Dubelaar, T.G. Nijland, Early Cretaceous Obernkirchen and Bentheim Sandstones from Germany used as dimension stone in the Netherlands: geology, physical properties, architectural use and comparative weathering, Geol. Soc. London, Spec. Publ. 416 (2016) 163–181. https://doi.org/10.1144/SP416.13.

[38] M. Roveri, S. Goidanich, G. Dotelli, L. Toniolo, Semi-empirical models to describe the absorption of liquid water in natural stones employed in built heritage before and after the application of water repellent treatments, Constr. Build. Mater. 241 (2020) 117918. https://doi.org/10.1016/j.conbuildmat.2019.117918.

[39] X. XIAO, J. LIU, Synthesis and Characterization of Fluorine-containing Polyacrylate Emulsion with Core-Shell Structure, Chinese J. Chem. Eng. 16 (2008) 626–630. https://doi.org/10.1016/S1004-9541(08)60131-7.

[40] J.W. Ha, I.J. Park, D.K. Kim, J.H. Kim, S.B. Lee, Surface properties of core-shell particles containing perfluoroalkyl acrylate in shell, Surf. Sci. 532–535 (2003) 328–333. https://doi.org/10.1016/S0039-6028(03)00463-1.

[41] S. Cheng, Y. Chen, Z. Chen, Core-shell latex containing fluorinated polymer rich in shell, J. Appl. Polym. Sci. 85 (2002) 1147–1153. https://doi.org/10.1002/app.10622.

[42] C. Zhang, Y. Chen, Investigation of fluorinated polyacrylate latex with core-shell structure, Polym. Int. 54 (2005) 1027–1033. https://doi.org/10.1002/pi.1803.

[43] X. Cui, S. Zhong, H. Wang, Synthesis and characterization of emulsifier-free core-shell fluorine-containing polyacrylate latex, Colloids Surfaces A Physicochem. Eng. Asp. 303 (2007) 173–178. https://doi.org/10.1016/j.colsurfa.2007.03.037.

[44] M. Li, X.S. Lin, X.Y. Li, H.Q. Wang, Preparation and property study of core-shell ambient-temperature crosslinkable polyacrylate binder, in: Appl. Mech. Mater., Trans

Tech Publ, 2014: pp. 3–6. https://doi.org/10.4028/www.scientific.net/AMM.469.3.

[45] J. De Zhang, M.J. Yang, Y.R. Zhu, H. Yang, Synthesis and characterization of crosslinkable latex with interpenetrating network structure based on polystyrene and polyacrylate, Polym. Int. 55 (2006) 951–960. https://doi.org/10.1002/pi.2056.

[46] N. Kessel, D.R. Illsley, J.L. Keddie, The diacetone acrylamide crosslinking reaction and its influence on the film formation of an acrylic latex, J. Coatings Technol. Res. 5 (2008) 285–297. https://doi.org/10.1007/s11998-008-9096-6.

[47] A. Murru, R. Fort, Diammonium hydrogen phosphate (DAP) as a consolidant in carbonate stones: Impact of application methods on effectiveness, J. Cult. Herit. 42 (2020) 45–55. https://doi.org/10.1016/j.culher.2019.09.003.

[48] E. Maire, P.J. Withers, Quantitative X-ray tomography, Int. Mater. Rev. 59 (2014) 1–43. https://doi.org/10.1179/1743280413Y.0000000023.

[49] F. Brun, S. Pacilè, A. Accardo, G. Kourousias, D. Dreossi, L. Mancini, G. Tromba, R. Pugliese, Enhanced and Flexible Software Tools for X-ray Computed Tomography at the Italian Synchrotron Radiation Facility Elettra, Fundam. Informaticae. 141 (2015) 233–243. https://doi.org/10.3233/FI-2015-1273.

[50] F. Brun, L. Massimi, M. Fratini, D. Dreossi, F. Billé, A. Accardo, R. Pugliese, A. Cedola, SYRMEP Tomo Project: a graphical user interface for customizing CT reconstruction workflows, Adv. Struct. Chem. Imaging. 3 (2017) 4. https://doi.org/10.1186/s40679-016-0036-8.

[51] A.C. Kak, M. Slaney, Tomographic Imaging with Diffracting Sources, in: Princ. Comput. Tomogr. Imaging, Society for Industrial and Applied Mathematics, 2001: pp. 203–274. https://doi.org/10.1137/1.9780898719277.fm.

[52] J. Schindelin, I. Arganda-Carreras, E. Frise, V. Kaynig, M. Longair, T. Pietzsch, S. Preibisch, C. Rueden, S. Saalfeld, B. Schmid, J.-Y. Tinevez, D.J. White, V. Hartenstein, K. Eliceiri, P. Tomancak, A. Cardona, Fiji: an open-source platform for biological-image analysis, Nat. Methods. 9 (2012) 676–682. https://doi.org/10.1038/nmeth.2019.

[53] F. Brun, L. Mancini, P. Kasae, S. Favretto, D. Dreossi, G. Tromba, Pore3D: A software library for quantitative analysis of porous media, Nucl. Instruments Methods Phys. Res. Sect. A Accel. Spectrometers, Detect. Assoc. Equip. 615 (2010) 326–332. https://doi.org/10.1016/j.nima.2010.02.063.

[54] J.D. Kubicki, L.M. Schroeter, M.J. Itoh, B.N. Nguyen, S.E. Apitz, Attenuated total reflectance Fourier-transform infrared spectroscopy of carboxylic acids adsorbed onto mineral surfaces, Geochim. Cosmochim. Acta. 63 (1999) 2709–2725. https://doi.org/10.1016/S0016-7037(99)00194-5.

[55] L. Zarybnicka, J. Machotová, P. Mácová, D. Machová, A. Viani, Design of polymeric binders to improve the properties of magnesium phosphate cement, Constr. Build. Mater. 290 (2021) 123202. https://doi.org/10.1016/j.conbuildmat.2021.123202.